Charge-transport properties of dendritic germanium thin films

K. M. Lui, W. H. Wong, and K. P. Chik
Department of Physics, The Chinese University of Hong Kong, Shatin, New Territories, Hong Kong, China
(Received 11 May 1998)

The charge transport properties of dendritic Ge thin films on glass substrates before and after postannealing have been studied by the methods of temperature-dependent electrical conductivity measurements and temperature-dependent Hall mobility measurements. Results showed that the dendritic structure is consistent with a crystalline matrix consisting of a high density of structural defects that cause degenerate conduction at high temperatures. Postannealing of the as-prepared samples at a temperature $\geqslant$570 °C for 2 h succeeded in converting the degenerate conduction into a nondegenerate one. All the samples were found to be *p*-type in the low-temperature regime (20–100 K). The origin of the acceptorlike states within the forbidden gap was suggested to arise from dangling-bond-related defects, which could be partially removed by the prolonged annealing. Hall mobility (μ_H) data in the temperature range from 20 to 300 K revealed that the charge carriers were subjected to two kinds of scattering mechanisms. At low temperatures, ionized center scattering was found to dominate and μ_H showed a T^{α} dependence, where α is a positive constant; while at higher temperatures μ_H was found to vary as $T^{-0.5}$ rather than the expected $T^{-3/2}$ dependence. This was explained in terms of a structural-imperfection-limited mean free path of the charge carriers. [S0163-1829(98)06648-X]

I. INTRODUCTION

Recently, it has been shown that giant dendritic crystallization of amorphous germanium (a-Ge) thin films on Corning glass substrates can result from *in situ* thermal pulse annealing;[1] yet under stringent conditions at which kinetics plays an overwhelming role. A former estimation has shown that the growth velocity of the dendrites is at least an order of magnitude greater than that of the solid phase epitaxial regrowth of Ge along any crystallographic direction.[1,2] Since the maximum temperature attained by the thermal pulse was well below the equilibrium melting temperature of Ge, this leads to the conjecture that the transformation may have passed through an intermediate semiconductive liquid phase[1,3] under the action of the thermal transient and crystallization proceeded at a great velocity. As a result, the resultant films are expected to consist of a vast amount of structural defects of both point and extended types. On the other hand, the dendritic Ge thin film provides an ideal system for studying charge transport phenomena in a highly defective crystalline matrix of the semiconductor. The dendritic structure is in itself distinctive because a high density of structural defects is generated upon the course of crystallization. Consequently, they are distributed throughout the entire volume of the samples. Besides, as no foreign atom is intentionally introduced to create the defects, this greatly suppresses the intervention of charge transport inside the samples by impurity atoms, the influences of which were shown to depend markedly on their chemical natures at low temperatures.[4] Most interestingly, dendritic Ge thin films should reveal transport properties different from those of typical granular microcrystalline structures. This arises from the fact that the dendritic grains are usually in the sizes of 10^1-10^4 μm, being about several orders of magnitude larger than those of typical micrograins.[5–9] The large grain volume to grain boundary area ratio makes the grain boundary potential barrier[5,10] no longer the first-order effect controlling the charge transport in the films. In this study, the temperature dependences of electrical conductivity and Hall mobility of dendritic Ge thin films are reported and interpreted within the framework of existing theories of conduction in semiconductors, with particular attention being paid to different scattering mechanisms of the charge carriers at low and moderate temperatures.

II. THEORY

In this section, we shall briefly review expressions for the temperature dependence of electrical drift mobility μ for a system of nondegenerate charge carriers, whose mean free paths are finite due to different scattering processes. Special attention will be paid to the scattering due to ionized centers, which was found to be the dominant process in the dendritic thin films at low temperatures. μ is considered because it is related to the Hall mobility (μ_H), which was actually measured in the present study, via a proportionality constant of the order of unity[11] for cases departing not too far from nondegenerate situations. In addition, μ and μ_H for degenerate systems will also be discussed.

A. General expression of μ

By using the relaxation time approximation, it is well known that for a system of charge carriers, say, holes under the perturbation of a uniform electric field in the x direction, the electrical conductivity at steady state can be written as[12]

$$\sigma = \frac{-e^2}{m^*} \int_{-\infty}^{0} \tau \left(\frac{\partial f}{\partial v_x} \right) v_x g(\epsilon) d\epsilon, \tag{1}$$

where e is the electronic charge, m^* the conductivity effective hole mass, τ the mean free time, f the occupation function of holes, v_x the x component of the velocity v of a hole with an energy $|\epsilon|$, and g the density of states function. For

nondegenerate cases, we can make use of the Boltzmann statistics and adopt the parabolic energy band scheme to obtain

$$\sigma = \frac{4ne^2}{3\pi^{1/2}m^*} \int_{-\infty}^{0} \tau(-\eta)^{3/2}\exp(\eta)d\eta, \tag{2}$$

where η equals ϵ/kT, k the Boltzmann constant, n the hole density, and T the absolute temperature. The mean free time τ can be defined as

$$\tau \equiv l(\epsilon,T)/v, \tag{3}$$

where l is the mean free path of a charge carrier with a velocity v. Since $v=(2kT/m^*)^{1/2}(-\eta)^{1/2}$ and $\sigma = n\mu e$, we have

$$\mu = \frac{4e}{3(2\pi m^* k)^{1/2}} \frac{1}{T^{1/2}} \int_{-\infty}^{0} l(-\eta)\exp(\eta)d\eta. \tag{4}$$

In order to get the temperature dependence of μ, hence μ_H, one has to know both the temperature dependence and energy dependence of l.

The relaxation time approximation assumes that the energy loss per collision must be small compared with the total energy of the charge carriers. Physically, this amounts to the idea that the energy distribution of the charge carriers should not be drastically changed by scatterings and once the perturbing field is turned off, the original energy distribution will be restored in a time of the order of τ. At low temperatures, while the average energy of the charge carriers is of the order of $\sim kT$, the average energy associating with optical phonons is of the order of $\sim k\theta_D$, where θ_D is the Debye temperature. Thus the energy change in the charge carriers will not be small in the case of optical phonon scatterings. Notwithstanding, since the density of optical phonons varies as $\exp(-\theta_D/T)$ and in the present study, the Hall measurements were made in the temperature range from 20 to 300 K, which lies below the Debye temperature $\simeq$377 K of Ge,[13] we expect that the contribution of optical phonons to the scattering of charge carriers in our case is small and the use of the relaxation time approximation should be legitimate.

B. μ resulting from ionized center scattering

The scattering of charge carriers by ionized centers is physically equivalent to the Rutherford scattering, i.e., a scattering process by the Coulomb field in a dielectric medium of permittivity ε. Although the mean free path $l_{\rm ion}$ resulting from the Rutherford scattering does not explicitly depend on temperature, it is proportional to the square of the energy of the charge carriers (i.e., $l_{\rm ion} \propto \epsilon^2$). Inserting this fact into Eq. (4), we get $\mu \propto T^{3/2}$. While this is essentially correct, by assuming the Coulomb field of an ionized center ceases to be effective at a radius $r_m \simeq N_i^{-1/3}/2$, where N_i is the number of ionized centers per unit volume, and r_m is equal to half the mean distance between centers, Conwell and Weisskopf[14] suggested that the electrical drift mobility ($\mu_{\rm ion}$) due to ionized center scattering is given by

$$\mu_{\rm ion} = \frac{CT^{3/2}N_i^{-1}}{\ln[1+DN_i^{-2/3}T^2]}. \tag{5}$$

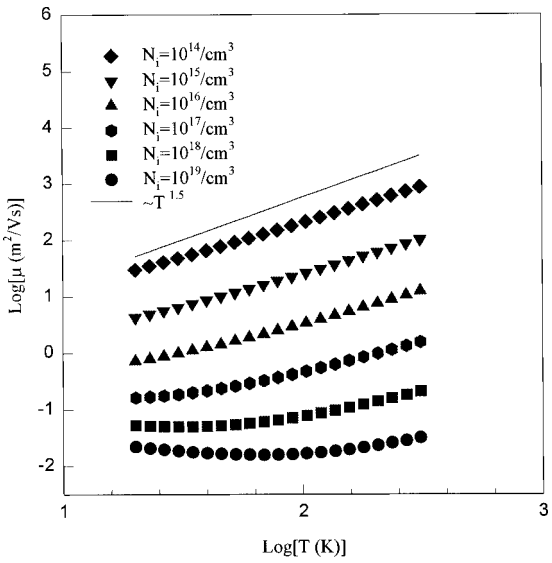

FIG. 1. Numerical calculations of the Conwell-Weisskopf formula for ionized center scattering.

Here

$$C \equiv \frac{64\pi^{1/2}\varepsilon^2(2k)^{3/2}}{Z^2e^3(m^*)^{1/2}} \quad \text{and} \quad D \equiv \left(\frac{12\pi\varepsilon k}{Ze^2}\right)^2.$$

Equation (5) can be interpreted as follows. At moderate temperatures, the logarithmic term varies slowly with temperature. Hence $\mu_{\rm ion}$ essentially has a $T^{3/2}$ dependence. However, when the number of scattering centers is large such that for any finite temperature $DN_i^{-2/3}T^2 \ll 1$, we have $\mu_{\rm ion} = (C/D)N_i^{-1/3}T^{-1/2}$. Thus a transition from the $T^{3/2}$ to $T^{-1/2}$ dependence should be observed as N_i increases. On the other hand, for a given N_i, at a low enough temperature such that $T \ll N_i^{1/3}D^{-1/2}$, a transition from the $T^{3/2}$ to $T^{-1/2}$ dependence should again be observed. Therefore, by inspecting the temperature of this transition, relative concentrations of ionized centers in different samples can be inferred qualitatively. Figure 1 shows some numerical calculations of Eq. (5) using the following values for the parameters:

$\varepsilon = 16\varepsilon_0 = 1.417\times10^{-10}$ F/m for Ge (Ref. 15),

$m^* = 0.25m_e = 2.28\times10^{-31}$ kg for holes of Ge (Ref. 15),

$Z=1$ for singly ionized centers,

$k = 1.38\times10^{-23}$ J/K,

$e = 1.6\times10^{-19}$ C.

From Fig. 1, the following can be seen: (1) The magnitude of $\mu_{\rm ion}$ decreases with increasing N_i for any temperature. (2) At low N_i, the curve is almost a straight line with a slope approaching 1.5. When N_i increases beyond a certain value, the curve bends up at low enough temperatures. The higher the N_i value, the stronger the bending. This bending is a result of the transition from $T^{3/2}$ to $T^{-1/2}$ dependence of $\mu_{\rm ion}$ as the temperature is lowered. It should be noted that in the above calculations the density of ionized centers has been assumed to be temperature independent in evaluating the temperature

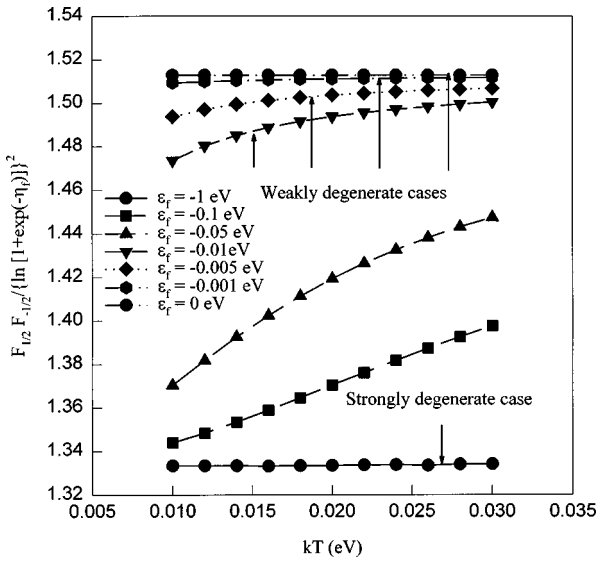

FIG. 2. Numerical evaluation of $F_{1/2}F_{-1/2}/\{\ln[1+\exp(-\epsilon_f/kT)]\}^2$ for different positions of Fermi levels. Note the valence band top is chosen as a reference level and is assigned to be zero. The temperature range is from 116 K to 348 K.

dependence of mobility for a particular N_i. Nevertheless, even if the ionization process is not complete at the lower temperatures and still goes on as the temperature increases, it can be shown that the general trend of the curves for the same set of final N_i values will not be significantly altered for ionization energies up to 0.015 eV (Ref. 16) (a typical value for acceptor ionization in Ge), provided that the assumption of a single scattering event[14] for each charge carrier is still valid.

C. μ and μ_H for degenerate cases

By assuming the mean free path l to be independent of energy and $\tau \propto |\epsilon|^{-1/2}$ as above, for degenerate cases, it can be shown that[17]

$$\mu_H \propto \frac{F_{1/2}F_{-1/2}}{\{\ln[1+\exp(-\epsilon_f/kT)]\}^2}\,\frac{l}{T^{1/2}}. \tag{6}$$

The definitions of the symbols are the same as above, with ϵ_f the Fermi level, and $F_{1/2}$ and $F_{-1/2}$ the well-known Fermi integrals for holes. Thus a change in the *temperature dependence* of μ_H from Eq. (4) should not be expected if $F_{1/2}F_{-1/2}/\{\ln[1+\exp(-\epsilon_f/kT)]\}^2$ depends weakly on temperature. This expression has been computed for the temperature range from 116 to 348 K for different positions of Fermi levels, corresponding to different degrees of degeneracy. Results are summarized in Fig. 2. It can be seen that for most cases the expression shows a variation of far less than 6% in its numerical value. Therefore, $F_{1/2}F_{-1/2}/\{\ln[1+\exp(-\epsilon_f/kT)]\}^2$ is practically insensitive to temperature in the above temperature range. Consequently, for an energy-independent mean free path, μ and μ_H should retain the temperature dependence given by Eq. (4).

III. SAMPLE PREPARATION AND EXPERIMENTAL METHODS

Amorphous-germanium (a-Ge) thin films were electron beam evaporated onto Corning 7059 glass substrates in a conventional high vacuum system. The base pressure was evacuated to $\simeq 2\times10^{-7}$ Torr prior to deposition. During deposition, the pressure within the chamber would not exceed $\simeq 2\times10^{-6}$ Torr. The thickness of the samples was $\simeq$5000 Å with a coating rate of $\simeq$5 Å/s, being monitored by a thickness quartz sensor. The substrate temperature was not controlled and deliberately rose to a maximum of 130 °C. *In situ* crystallization of the as-deposited a-Ge thin films were immediately induced by a home-built thermal pulse furnace (TPF) inside the vacuum chamber without breaking the vacuum. The TPF consists of six 1000-W halogen lamps, being divided into an upper and a lower half. When placed in the assigned position, the samples should sit halfway between the two lines of halogen lamps and will be subjected to $<10^2$ W/cm^2 broadband incoherent irradiation. The duration (t_e) of each thermal pulse was recorded by a digital oscilloscope (Thurby-Thandar SM620), which gives an uncertainty of $\pm$0.05 s. The thermal profile in the neighborhood of the substrates was probed by a pair of chromel-alumel (K-type) thermocouples and was recorded for each thermal pulse by an X-t plotter. This provides an indication on the heating rate of the thermal pulse as well as on the maximum temperature (T_m) reached by the system. In this study, the heating rate of the thermal pulse was $>$100 °C/s, with t_e and T_m being $\simeq$3.22 s and $\simeq$577 °C, respectively. The surface morphology of the as-prepared samples was examined by atomic force microscopy (Nanoscope III), the depth and transverse resolution of which is 0.1 and 10 nm, respectively. Postannealing of four batches of samples were done isochronally in a regulated furnace at 459, 560, 570, and 580 °C, respectively, each with an annealing time of 2 h. During annealing, the sample surface was protected by a continuous flow of normal grade (99.9%) nitrogen gas, purified first by passing through a trap immersed in liquid nitrogen before entering the annealing chamber. Electrical conductivity measurements were carried out inside a vacuum chamber of $\simeq 10^{-6}$ Torr. Thin copper wire electrodes were pasted onto the samples with silver paste. A current of $\simeq$0.1 mA from a constant current source was sent through the sample. The voltage drop across the sample was recorded by an electrometer (Keithley 617). The measuring process started at 250 °C with a ramping down rate of $\simeq$0.5 °C/min until 30 °C was reached. Hall mobility was measured by the van der Pauw technique with the samples in square geometry. Measurements were carried out in an argon atmosphere in order to eliminate any thermal gradient within the sample and to avoid condensation at low temperatures. The measuring temperature was regulated by a temperature controller in conjunction with a resistive heater and a cold head connected to a cryostat. Before each experiment, the Ohmicity of all the contacts were checked by inspecting the linearity of their respective voltage-current curves in all permutations at 20 K. For sheet conductance measurements, no magnetic field was applied. A constant field of 3500 G was maintained during the measurements of Hall voltages. The wait-state was always allowed for whenever there was a change in any experimental parameter, including both reversals of magnetic field and current directions.

IV. RESULTS

The transport properties of dendritic Ge films on glass substrates (Fig. 3) were studied before and after postanneal-

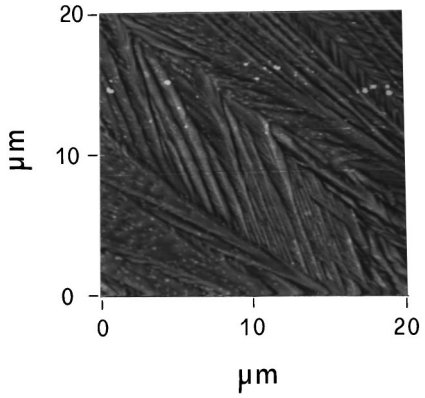

FIG. 3. A typical AFM micrograph of the dendritic Ge samples.

ing. Electrical conductivity was measured in the temperature range from 523 to 303 K. Both sheet conductance and Hall mobility were measured from 300 down to 20 K. *P*-type conduction was found for all the samples at low temperatures. The carrier concentrations at 300 K of the as-prepared and 580 °C-annealed samples were estimated to be $\simeq 10^{19}$ and 10^{17} cm^{-3}, respectively. Results of the above measurements indicated a high density of structural defects present in the dendritic films. Postannealing succeeded in removing part of them and thus gave control over the degeneracy of the samples.

A. Conductivity in the temperature range 523–303 K

Figure 4 summarizes the results. For the as-prepared sample, conductivity increases with decreasing temperature. This is a typical behavior of a degenerate semiconductor. The effect of annealing is to lower the conductivity and to convert the degenerate behavior into a nondegenerate one. Conduction in the sample annealed at 580 °C for 2 h is evidently nondegenerate with an activation energy of 0.023 eV, which is much smaller than half of the bandgap energy in the bulk (i.e., 0.335 eV).[15] Therefore, the conduction is expected to involve states within the forbidden gap.

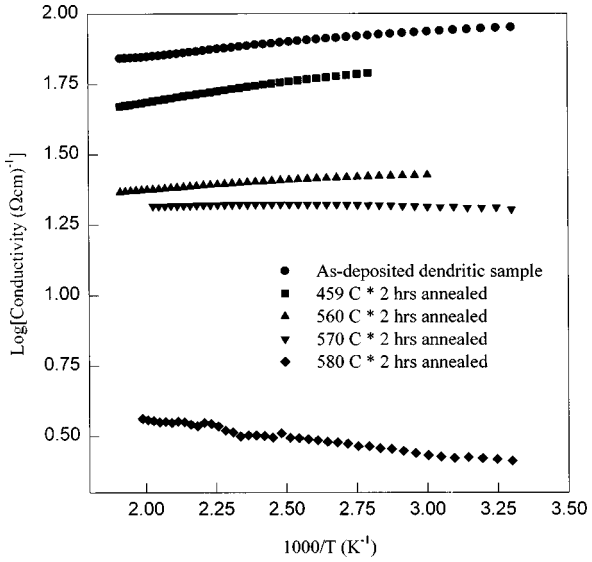

FIG. 4. Electrical conductivity measurements in the high temperature range (523 K to 303 K) for samples subjected to different post-annealing treatments.

B. Sheet conductance in the temperature range 300–20 K

Results are shown in Figs. 5(a)–5(d).

1. As-prepared sample

Three kinds of conduction phenomena can be identified. For temperatures above ≃100 K, conduction is degenerate in agreement with the results in Sec. IV A. Below ≃100 K, the sheet conductance can be described by the following equation:

$$G_1 = 4.7\times 10^{-3}\exp(-2.8\times 10^{-4}\ \text{eV}/kT) + 4.53\times 10^{-3} \times \exp(-5.6\times 10^{-5}\ \text{eV}/kT)\ \ \Omega^{-1}/\square. \quad (7)$$

2. Sample annealed at 459 °C for 2 h

Above ≃100 K, the sample is again degenerate. Below ≃100 K, the sheet conductance can be described by the following equation:

$$G_2 = 3.6\times 10^{-3}\exp(-9.5\times 10^{-4}\ \text{eV}/kT) + 2.9\times 10^{-3} \times \exp(-4.1\times 10^{-5}\ \text{eV}/kT)\ \ \Omega^{-1}/\square. \quad (8)$$

3. Sample annealed at 570 °C for 2 h

In the whole temperature range of study, the sheet conductance can be described by the following equation:

$$G_3 = 1.3\times 10^{-3}\exp(-7.3\times 10^{-3}\ \text{eV}/kT) + 4.9\times 10^{-4} \times \exp(-4.0\times 10^{-4}\ \text{eV}/kT)\ \ \Omega^{-1}/\square. \quad (9)$$

4. Sample annealed at 580 °C for 2 h

$$G_4 = 2.5\times 10^{-3}\exp(-0.023\ \text{eV}/kT) + 4.5\times 10^{-4} \times \exp(-5.9\times 10^{-3}\ \text{eV}/kT)\ \ \Omega^{-1}/\square. \quad (10)$$

The activation energy in the first term agrees with the value obtained in the high-temperature range.

C. Hall mobility in the temperature range from 300 to 20 K

Results are shown in Figs. 6(a)–6(d). A change in scattering mechanisms is evident in all the samples as the temperature is lowered. In general, the slope of the $\log_{10}\mu_H - \log_{10} T$ plot changes from negative on the high-temperature side to positive on the low temperature side and in some cases the curve bends up slightly when the temperature is further lowered. A conversion temperature T_c can be identified as at which a change in the sign of the slope occurs. It is observed that T_c varies with the annealing conditions. Table I summarizes these results as well as the activation energy for extrinsic conduction. It can be seen that, for $T<T_c$, as the annealing temperature increases μ_H gradually changes from $\sim T^{0.09}$ to $\sim T^{1.4}$; whereas for $T>T_c$, μ_H remains $\sim T^{-0.5}$. Furthermore, T_c shows a correlation with the activation energy E_a' for extrinsic conduction. It is found that T_c increases along with E_a'.

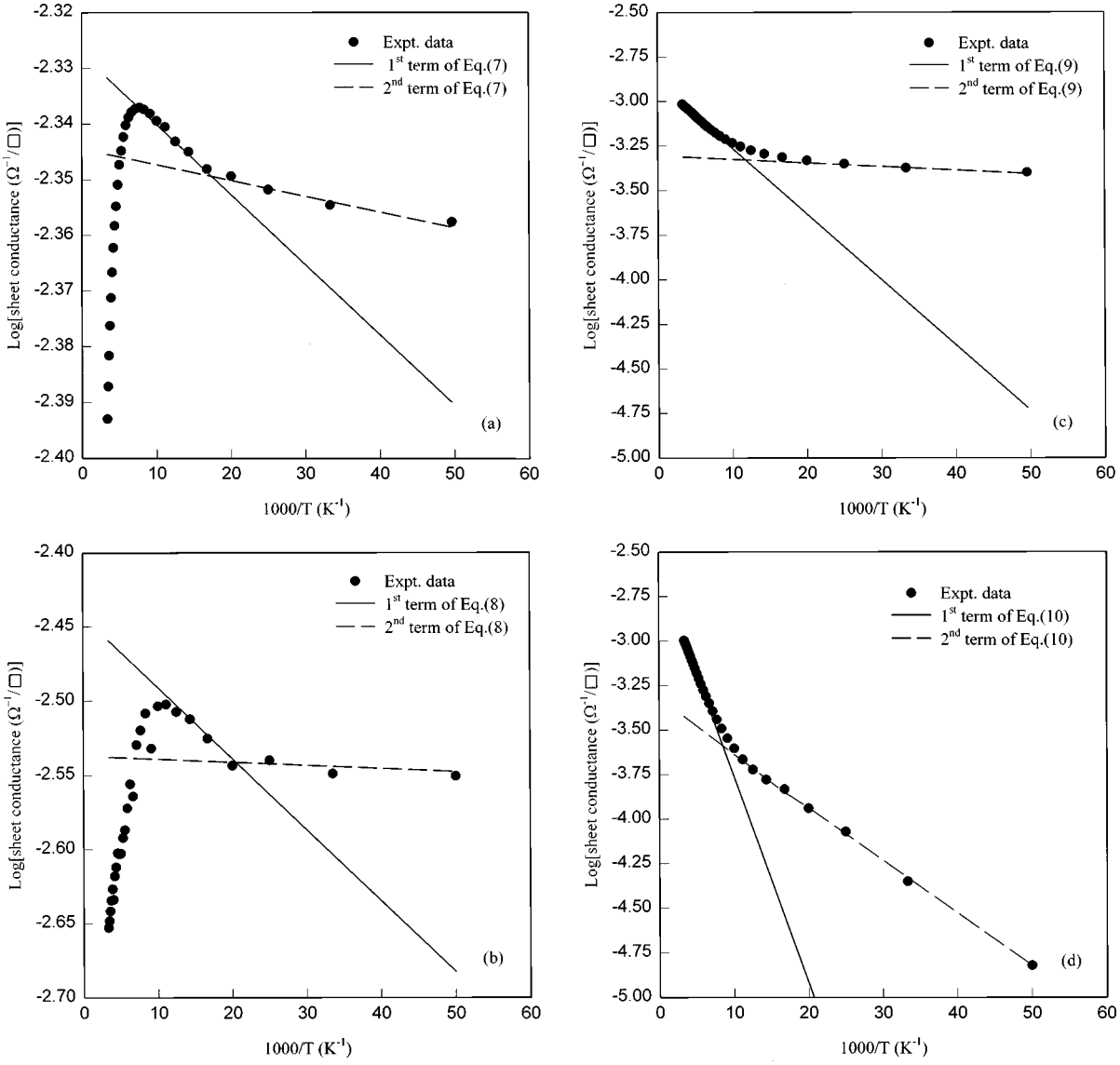

FIG. 5. (a) Sheet conductance of the as-prepared sample in the temperature range 300–20 K. (b) Sheet conductance of the sample postannealed at 459 °C for 2 h in the temperature range 300–20 K. (c) Sheet conductance of the sample postannealed at 570 °C for 2 h in the temperature range 300–20 K. (d) Sheet conductance of the sample postannealed at 580 °C for 2 h in the temperature range 300–20 K.

V. DISCUSSIONS

A. Temperature dependence of electrical conductivity

The most astonishing result is that the samples showed degenerate behavior above a certain temperature unless they were annealed at a sufficiently high temperature. The as-prepared film and the one annealed at 459 °C became degenerate around 100 K, but the ones annealed at 570 and 580 °C were nondegenerate up to more than 300 K. It is thus clear that degeneracy in the films can be removed by prolonged high temperature annealing. Since our samples were not intentionally doped, degeneracy could not be due to foreign dopants. In view of the dendritic nature of the samples, it is possible that the degenerate conducting behavior may arise from structural defects such as dangling bonds on grain boundaries and in network of dislocations[18] since these structural defects can be partially removed by annealing.

Evidence of a high density of acceptor levels (since the samples were *p*-type at sufficiently low temperatures) in the samples can be found in the conducting behavior at low temperatures. In the low-temperature range, the nondegenerate conduction can be generally described by a two-channel conduction mechanism according to the equation

$$G = G' \exp(-E_a'/kT) + G'' \exp(-E_a''/kT), \qquad (11)$$

where G' and G'' are the preexponential factors that weakly depend on temperature, E_a' and E_a'' the activation energies for conductions, k the Boltzmann factor, and T is the absolute temperature.

The first term resembles the conventional thermally activated extrinsic conduction process, yet instead of foreign dopants, intrinsic structural defects are involved here. The very small activation energy of the second term is typical for phonon-assisted nearest-neighbor-hopping, which is a quantum-mechanical tunneling of the charge carriers among localized states. Such a hopping phenomenon is usually observed in heavily doped or amorphous semiconductors,[19] which assume a high density of localized states within the

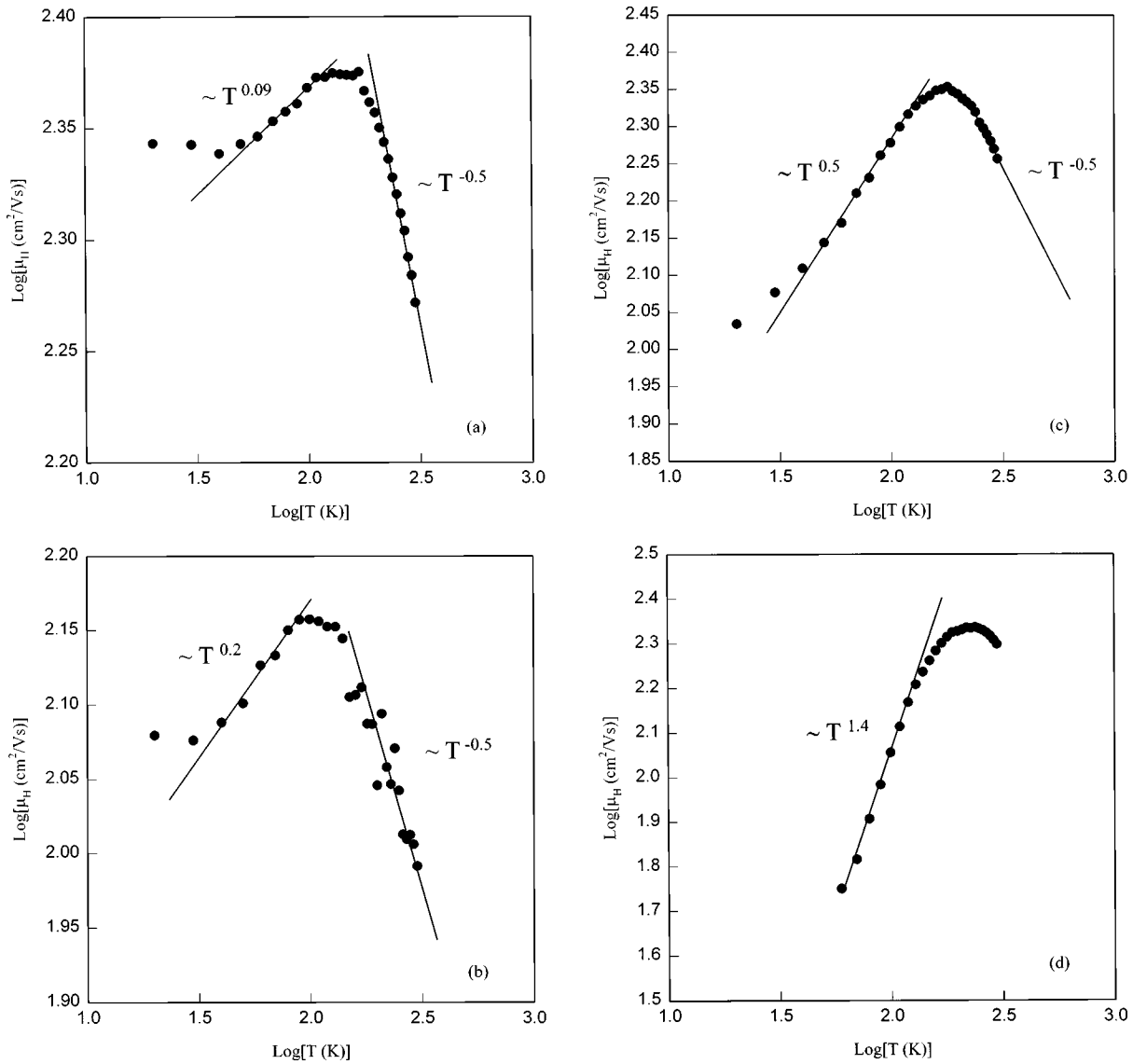

FIG. 6. (a) Hall mobility measurement for the as-prepared sample in the temperature range 300–20 K. (b) Hall mobility measurement for the sample postannealed at 459 °C for 2 h in the temperature range 300–20 K. (c) Hall mobility measurement for the sample postannealed at 570 °C for 2 h in the temperature range 300–20 K. (d) Hall mobility measurement for the sample postannealed at 580 °C for 2 h in the temperature range 300–20 K.

forbidden gap, at low temperatures and is thus consistent with our view presented above.

Thus our picture will be that structural defects provide the dendritic films with a high density of acceptor levels, leading to the *p*-type behavior observed in the Hall measurements. In the as-prepared and low temperature annealed samples, the density of structural defects is expected to be higher. Thus degenerate conduction occurred at a relatively low temperature around 100 K. The absence of degenerate behavior in samples annealed above 570 °C indicates that a considerable amount of structural defects have been annealed out.

TABLE I. A summary on the Hall mobility results, the conversion temperature T_c for the transition in scattering mechanisms, and the activation energy for extrinsic conduction, for samples experiencing different postannealing treatments.

Sample	$\mu_H\ (T<T_c)$	$\mu_H\ (T>T_c)$	T_c (K)	$E_a'\times 10^4$ (eV)
As-prepared	$\sim T^{0.09}$	$\sim T^{-0.5}$	143	2.8
459 °C annealed	$\sim T^{0.2}$	$\sim T^{-0.5}$	143	9.5
570 °C annealed	$\sim T^{0.5}$	$\sim T^{-0.5}$	182	73.0
580 °C annealed	$\sim T^{1.4}$		241	230.0

Further evidence for the elimination of structural defects by annealing is provided by the observation that the activation energy E_a' for conduction increases with an increase in the annealing temperature (Table I). According to Debye and Conwell,[20] the activation energy of an acceptor can depend on the density of ionized acceptors as

$$E_A = E_A^0\left[1-\left(\frac{N_A^-}{N_{\rm crit}}\right)^{1/3}\right], \tag{12}$$

where E_A is the activation energy of an acceptor, E_A^0 a constant, N_A^- the average density of the ionized acceptors, and $N_{\rm crit}$ the critical concentration.

From the above equation, one sees that as the concentration of ionized acceptors increases, the activation energy for acceptors decreases and once N_A^- is above a critical value $N_{\rm crit}$, no thermal excitation is necessary for the holes associated with the acceptors and the semiconductor becomes degenerate. In our case, the number of ionized acceptors depends on the number of acceptor levels, which in turns depends on the amount of structural defects (dangling bonds). The as-prepared sample should house the largest amount of defects, as evident from the degenerate conduction behavior in 303 to 523 K. Thermal annealing has been known as a means to reduce dangling bond defects,[21] and the density of acceptor levels should reach a minimum for the sample annealed at 580 °C. According to Eq. (12), this type of sample should show the highest activation energy for extrinsic conduction. Indeed, the activation energy was found to be $\simeq 10^{-2}$ eV, nearly two orders of magnitude higher than that of the as-prepared sample.

The physical reason for the above phenomenon may be as follows. Since dangling bond defects on grain boundaries or in a network of dislocations are localized in real space, upon pairing up with an electron from the valence band, the Ge atoms associated with the dangling bonds will be negatively charged, creating a space-charge region. The free hole gas that is attracted to this region will screen the Coulomb field of the nearby acceptors[22] (i.e., neutral atoms with dangling bonds or in other words, atoms with unionized holes), resulting in a decrease in the activation energy. The effectiveness of this screening effect, and thus the amount of decrease in the activation energy surely depends on the density of the free hole gas, hence on the density of acceptors (dangling bonds).

B. Temperature-dependent Hall mobility measurements

Hall mobility (μ_H) measurements have been carried out for samples subjected to different annealing temperatures. In the present study, $\mu_H(T)$ is governed by two scattering mechanisms, with each dominating at a different temperature region. A temperature of conversion T_c can be designated to signify the transition from one to another. For $T<T_c$, $\mu_H(T)$ varies as T^{α}, where α is a positive constant; while for $T>T_c$, μ_H shows a dependence of $\sim T^{-0.5}$ for all of the samples. The absolute value of T_c is noted to correlate with the activation energy E_a' for extrinsic conduction.

1. For $T<T_c$

For $T<T_c$, μ_H is seen to vary as T^{α}, and α takes values from 0.09 to 1.4 (Table I), increasing along with an increase in the annealing temperature. The value 1.4 agrees well with the value 1.5 predicted by the formula of Conwell and Weisskopf for ionized center scattering neither too low in measuring temperature nor too high in ionized center density (N_i). The gradual increase in α can be readily explained by noting that upon annealing N_i in the sample is expected to decrease as discussed above. The argument of a smaller N_i gives a higher α can be qualitatively seen from the numerical calculations of the ionized center scattering model. As can be seen in Fig. 1, as N_i increases, the slope α measured below $\simeq$100 K in the $\log_{10}\mu$-$\log_{10}T$ plot decreases. The decrease of α along with an increase in N_i is due to the fact that a transition from the $T^{3/2}$ to the $T^{-1/2}$ dependence is taking place as the condition $DN_i^{-2/3}T^2 \ll 1$ becomes satisfied. Thus for a fixed measuring temperature T_f, the slope $\alpha(T_f)$ from the $\log_{10}\mu_H$-$\log_{10}T$ plot qualitatively reveals the relative N_i in the samples, being smaller for a larger N_i. This agrees with the fact that the as-prepared sample assumed the largest N_i showing the smallest α. Besides, the increasing curl-up of the experimental curves at even lower temperatures, which is also predicted by the model, for samples annealed below 580 °C supports the argument that N_i should decrease as annealing temperature increases.

2. For $T>T_c$

It is interesting to note that for $T>T_c$, μ_H varies as $T^{-0.5}$ rather than the expected $\sim T^{-1.5}$, or to be exact, $\sim T^{-2.3}$ for the scattering of holes by acoustic phonons in germanium.[23] In order to understand this $T^{-0.5}$ dependence, one has to consider the mean free path $\langle l\rangle$ of the charge carriers. Explicitly,[24]

$$1/\langle l\rangle = 1/\langle l_{\rm im}\rangle + 1/\langle l_{\rm ion}\rangle + 1/\langle l_{\rm ph}\rangle, \tag{13}$$

where $\langle l\rangle$ is the resultant averaged mean free path and $\langle l_{\rm im}\rangle, \langle l_{\rm ion}\rangle, \langle l_{\rm ph}\rangle$ are the ensemble-averaged mean free paths arising by structural imperfections, by ionized centers, and by acoustic phonons, respectively.

For ionized center scattering, although the mean free path given rise by the Rutherford scattering does not explicitly depend on temperature, it is proportional to the square of the energy of the charge carriers,[14]

$$\therefore \langle l_{\rm ion}\rangle \propto T^2. \tag{14}$$

Therefore, $\langle l_{\rm ion}\rangle$ should increase as temperature increases. While for phonon scattering, μ varies as $T^{-3/2}$,

$$\therefore \langle l_{\rm ph}\rangle \propto 1/T. \tag{15}$$

Thus we see that the significance of $\langle l_{\rm ion}\rangle$ should subside as compared to $\langle l_{\rm ph}\rangle$ when the temperature is sufficiently high. For $\langle l_{\rm im}\rangle$, since permanent imperfections of a crystal lattice should give rise to a mean free path independent of temperature and the energies of the charge carriers, $\langle l_{\rm im}\rangle$ ought to be a constant. Thus at high enough temperatures, we have

$$1/\langle l\rangle \simeq 1/\langle l_{\rm im}\rangle + 1/\langle l_{\rm ph}\rangle. \tag{16}$$

Now, we postulate that in the present experimental range $\langle l_{\rm im}\rangle \ll \langle l_{\rm ph}\rangle$. This may be justified by noting that dendritic Ge films consist of a vast amount of grain boundaries as observed from the atomic force microscopy (AFM) micrograph, and are expected to associate with a large amount of dislocations and point defects. These distortions in the crystal lattice surely shorten the mean free path of the charge carriers. As a result, l should be limited by $l_{\rm im}$. Since it is expected that the as-prepared and the low-temperature annealed samples are at most weakly degenerate upon approaching 300 K, the use of Boltzmann statistics, and hence Eq. (4) should not lead to an erroneous temperature dependence of the Hall mobility as evident from Fig. 2. By inserting $l \simeq l_{\rm im}$ into Eq. (4), a mobility $\mu \propto T^{-0.5}$ results in excellent agreement with the experimental findings.

The concept of a structural-imperfection-limited mean free path is also consistent with the observed correlation between T_c and the activation energy E_a' for extrinsic conduction. From Table I, it is observed that T_c increases along with an increase in the activation energy E_a'. It has been argued that E_a' should correlate with the density of structural defects within the samples. A higher E_a' implies a lower density of structural defects. In other words, a lower density of defects is seen to associate with a higher T_c. Now, fewer dangling bond related defects should be accompanied with a better crystal quality. Consequently, the mean free path $l_{\rm im}$ should increase, resulting in a conversion of scattering mechanism at a higher temperature as observed experimentally.

VI. CONCLUSIONS

To conclude, the transport properties of dendritic Ge films were studied by means of temperature-dependent electrical conductivity measurement from 20 to 523 K and temperature-dependent Hall measurement from 20 to 300 K. Results showed that the dendritic films consisted of a vast amount of structural defects that led to degenerate conduction at high temperatures and low Hall mobility ($\simeq 10^2$ cm^2/V s). All of the samples were found to be *p* type in the low-temperature regime. The origin of the acceptor levels in the forbidden gap is attributed to their originating from structural defects, a possible candidate of which is suggested to be dangling bonds in the dendritic crystals. Thermal annealing was shown to be capable of removing part of the defects. Hall mobility could be generally described by two scattering mechanisms. At low temperatures, ionized center scattering was found to dominate and to give rise to a T^{α} dependence of μ_H, where α is a positive constant whose magnitude depends on the amount of defects within the samples. At higher temperatures, μ_H was found to vary as $T^{-0.5}$ rather than the expected $T^{-3/2}$ dependence. This was explained in terms of a structural-imperfection-limited mean free path, which should be practically a constant, of the charge carriers.

[1] K. M. Lui, K. P. Chik, and J. B. Xu, J. Appl. Phys. **81**, 7757 (1997).

[2] L. Csepregi, R. P. Küllen, and J. W. Mayer, Solid State Commun. **21**, 1019 (1977).

[3] A. Kitagawa, S. Kanai, and M. Suzuki, J. Non-Cryst. Solids **164–166**, 239 (1993).

[4] V. I. Fistul', *Heavily Doped Semiconductors* (Plenum, New York, 1969), pp. 136–138.

[5] J. Y. W. Seto, J. Appl. Phys. **46**, 5247 (1975).

[6] I. W. Wu, A. Chiang, M. Fuse, L. Öveçoglu, and T. Y. Huang, J. Appl. Phys. **65**, 4036 (1989).

[7] J. S. Im and H. J. Kim, Appl. Phys. Lett. **64**, 2303 (1994).

[8] G. Baccarani, B. Ricco, and G. Spadini, J. Appl. Phys. **49**, 5565 (1978).

[9] M. K. Hatalis and D. W. Greve, J. Appl. Phys. **63**, 2260 (1988).

[10] S. N. Singh, R. Kishore, and P. K. Singh, J. Appl. Phys. **57**, 2793 (1985).

[11] E. H. Putley, *The Hall Effect and Related Phenomena* (Butterworth, London, 1960), p. 82.

[12] E. H. Putley, *The Hall Effect and Related Phenomena* (Ref. 11), p. 72.

[13] A. A. Bennett and D. E. Gray, American Institute of Physics Handbook, 3rd ed. (McGraw Hill, New York, 1972).

[14] E. Conwell and V. F. Weisskopf, Phys. Rev. **77**, 388 (1950).

[15] See, for example, S. M. Sze, *Physics of Semiconductor Devices*, 2nd ed. (Wiley, New York, 1981), p. 849.

[16] W. H. Wong and K. M. Lui (unpublished).

[17] E. H. Putley, *The Hall Effect and Related Phenomena* (Ref. 11), p. 86.

[18] N. F. Mott, Can. J. Phys. **34**, 1356 (1956).

[19] K. P. Chik and K. C. Koon, Philos. Mag. B **53**, 399 (1986).

[20] P. P. Debye and E. M. Conwell, Phys. Rev. **93**, 693 (1954).

[21] K. P. Chik, S. Y. Feng, and S. K. Poon, Solid State Commun. **33**, 1019 (1980).

[22] L. Pincherle, Proc. Phys. Soc. London, Sect. A **64**, 663 (1951).

[23] E. H. Putley, *The Hall Effect and Related Phenomena* (Ref. 11), p. 141.

[24] J. S. Blakemore, *Solid State Physics*, 2nd ed. (Cambridge University Press, New York, 1985), p. 331.